Surface residual stresses in multipass welds produced using low transformation temperature filler alloys

T. I. Ramjaun[a], H. J. Stone[a], L. Karlsson[b], M. Gharghouri[c], K. Dalaei[d], R. Moat[e], H. K. D. H. Bhadeshia[a]

[a]*Materials Science and Metallurgy, University of Cambridge, CB3 0FS, U.K.*

[b]*Engineering Science, University West, SE-461 86 Trollhättan, Sweden*

[c]*Canadian Neutron Beam Centre, Chalk River Laboratories, ON K0J 1J0, Canada*

[d]*ESAB AB, Lindholmsallen 9, 40277, Gothenburg, Sweden*

[e]*Materials Engineering, The Open University, Milton Keynes, MK7 6AA*

Abstract

Tensile residual stresses at the surface of welded components are known to compromise fatigue resistance through the accelerated initiation of microcracks, especially at the weld toe. Inducement of compression in these regions is a common technique employed to enhance fatigue performance. Transformation plasticity has been established as a viable method to generate such compressive residual stresses in steel welds and exploits the phase transformation in welding filler alloys, that transform at low temperature to compensate for accumulated thermal contraction strains. Neutron and X-ray diffraction have been used to determine the stress profiles that exist across the surface of plates welded with low transformation temperature welding alloys, with a particular focus on the stress at the weld toe. For the first time, near-surface neutron diffraction data have shown the extent of local stress variation at the critical, fusion boundary location. Compression was evident for the three measurement orientations at the fusion boundaries. Compressive longitudinal residual stresses and tensile transverse stresses were measured in the weld metal.

Keywords: transformation induced plasticity, martensite, residual stress, welding, neutron, X-ray, diffraction

Email address: `tir20@cam.ac.uk` (T. I. Ramjaun)

1. Introduction

The welded joints of engineering structures are often the features that limit both the service loads that can be tolerated and their fatigue life. Stress at the boundary between the weld metal and base material caused by geometrical changes coupled with local microstructural changes often leads to preferential crack initiation and fatigue failure at this site [1]. Susceptibility to microcrack initiation/propagation can be further exacerbated by tensile residual stresses in this region, which accumulate as a result of thermal contraction strains during cooling of the weld to ambient temperature.

In order to increase the longevity of welded components, post-weld treatments may be applied that are either mechanical or thermal in nature. Heat treatments are able to relax internal stresses while mechanical processes tend to impart compression into the component surface or modify the weld toe geometry to reduce stress concentration. As such treatments are typically costly or impractical it may be preferable to modify the welding process to minimise the occurrence of such stresses. One method proposed originally by Jones and Alberry [2], is to counter the thermally induced tensile stresses through exploitation of the strains associated with solid-state phase transformation of the weld filler. Application of this mechanism has led to a number of martensitic welding alloys being developed [3–11].

The transformation of austenite to martensite ($\gamma \rightarrow \alpha'$) is displacive and results in a shape deformation that is an invariant-plane strain with a large shear component [12]. The magnitude of the shear, in conjunction with a dilatational strain, is sufficient to not only cancel the tensile stresses, but even create compression in the weld metal. Detailed reviews of this mechanism and its influence on residual stresses in welds are available elsewhere [13, 14]. However, the beneficial effects of stress alleviation through transformation plasticity are dependant on the temperature at which the $\gamma \rightarrow \alpha'$ transformation occurs. If the transformation takes place above an optimal temperature, continued thermal contraction of the transformed product to ambient temperature leads to further accumulation of tensile stress. Thus, the initial benefits associated with the transformation are eliminated. To avoid this problem, the weld metal should be designed with a low martensite-start temperature (M_{S}), typically 200° C.

These low transformation temperature (LTT) welding alloys have proved effective in enhancing fatigue performance [15–20]. Although, judicious alloy design [21, 22] has been required in order to ensure that the carbon concentration is sufficiently low to avoid the embrittlement associated with hard martensite. The ability of LTT welding alloys to provide stress relief in single and multipass welds has also been established [23]. However, surface stress measurements obtained from synchrotron X-ray data are seemingly in contradiction with measurements made in the bulk using neutron diffraction, as they reveal tensile stress in the weld metal surface [24, 25].

In this work, near-surface neutron diffraction has been used to probe the residual stress state in the vicinity of the free surface and these results are

critically compared with residual stresses determined using X-ray diffraction. This study highlights the differences between the residual stresses at the surface and those in the bulk immediately below it, and serves to rationalise the apparent disparity between the residual stress data obtained with X-ray and neutron diffraction in previous studies.

2. Experimental Method

Three multipass welds were prepared from different welding consumables (LTT-1, LTT-2, HTT) deposited on a high strength ferritic steel plate (BP700) in order to measure the surface residual stresses. The specific welding procedures are given in Table 1, where LTT-1 and LTT-2 are martensitic stainless steel filler alloys with a low M_S, whilst HTT is a commercially available filler with a much higher M_S.

The equation by Steven & Haynes [26] was used to calculate the M_S of the welding fillers. Dilatometry was then used to verify the M_S of LTT-1 in its undiluted state. The measured value ($164\pm12\,°C$) was in agreement with the calculation. The welding alloy compositions and predicted martensite-start temperatures are shown in Table 2. LTT-2 is highly alloyed and was designed to compensate for dilution that occurs when the filler mixes with the base plate.

The base plate was prepared from $500 \times 150 \times 15$ mm sections, machined with a $60°$, 8 mm deep V-groove along the long direction and a root radius of 4 mm. The plates were clamped to the bench prior to mechanised gas-shielded metal arc welding (GMAW), which was performed horizontally in the down hand position, Fig. 1. All three welding alloys were deposited using metal-cored electrode wire, with an initial pre-heat of $50°C$ and an interpass temperature of 100–$125°C$. The heat input for the LTT and HTT welding alloys was ~1.0 and ~1.5 kJ mm^{-1} respectively. Details of the welding parameters are in Table 3. The mechanical properties of the welding fillers and base plate are in Table 4, the LTT data are measured values.

Welds L1 and H1 were produced to compare the surface stress distributions that develop during the cooling of a weld fabricated with an LTT filler with those that develop using a conventional filler, with the aim of correlating with fatigue data. Weld L2 was assessed to determine whether a single capping pass would be sufficient to provide the same surface stress distribution as a full LTT weld and hence, the desired fatigue improvement. Surface residual stresses were measured with both neutrons and X-rays.

2.1. Neutron Diffraction

The residual stresses measured using neutron diffraction were performed on the L3 beamline at the Canadian Neutron Beam Centre [27]. Strain scanning was performed across a plane perpendicular to the weld at the position along the sample shown in Fig. 2. Measurements were made at 0.15 and 2.5 mm below the top surface in the weld, heat-affected zone (HAZ)

and base plate to ascertain how the stresses vary with depth and across both sides of the weld.

A $0.3 \times 0.3 \times 1\,\text{mm}^3$ gauge volume was defined using $0.3\,\text{mm}$ wide slits on the incident and scattered sides, with a height limiter on the incident side for the longitudinal direction. The transverse and normal directions were measured using a gauge volume of $0.3 \times 0.3 \times 20\,\text{mm}^3$, with the long dimension of this volume parallel to the weld direction. The use of an elongated gauge volume in the welding direction was deemed appropriate as the residual stress is not expected to vary significantly along the central portion of the welded plates. The gauge volume selected was deemed to be the smallest possible that was capable of producing defined diffraction peaks. The centroid of the gauge volume could therefore be positioned at $0.15\,\text{mm}$ below the surface, whilst simultaneously avoiding partial-immersion errors. It was assumed that the principal stresses were parallel to the plate edges.

A monochromatic beam with a wavelength of $\sim$1.66 Åwas provided from a squeezed Ge (004) monochromator set to a take off angle $2\theta_\text{M} = 71.88\,^\circ$. The diffracted intensities were recorded on a position-sensitive detector. Measurements of the $\{211\}$ ferrite diffraction peak were performed around a scattering angle of $2\theta_\text{S} \approx 90^\circ$. The $\{211\}$ peak was selected as this reflection is known to accumulate only small compressive intergranular stresses following uniaxial tensile deformation [28, 29]. The stresses determined from the strains measured with this reflection and the appropriate diffraction elastic constant were therefore taken to be representative of the macroscopic residual stress.

2.2. Stress Analysis - Neutron Data

Assessing the stress distribution at the fusion boundary/weld-toe of the welded plates is necessary as this is the predominant site of failure during fatigue experiments. In order to achieve positional accuracy, the change in full width at half maximum (FWHM) across the fusion boundary at the plate surface was analysed in $0.25\,\text{mm}$ increments. The diffraction peak altered significantly when the gauge volume was totally immersed in the weld metal compared with the base plate and this effect was used to ascertain the fusion boundary positions at the surface.

Strain-free reference specimens ('comb' samples) were used to account for the effect of compositional variation between the filler alloy and base plate for the measured lattice spacings. These were produced as $3\,\text{mm}$ thick cross-sectional slices from the welded plate, Fig. 2, and further slotted at $3\,\text{mm}$ intervals along the transverse direction using wire electro-discharge machining (EDM), Fig. 3. Measurements were taken from the strain-free specimens at the same depths as that for the welded plate (0.15 and $2.5\,\text{mm}$ below the top surface) at the centre of each 'tooth'. However, as a result of the EDM cut positions, it was not possible to correlate the exact measurement locations for the comb with the welded plate in the transverse direction. Therefore, a function was used to fit the strain-free lattice spacing measurements at each depth. A linear interpolation was then performed

between the comb measurement positions to calculate the strain-free lattice spacings, $d_{0,hkl}$, for the relevant locations in the welded plates.

The elastic strain, ε_{hkl}, at each measurement location and direction was then found as follows:

$$\varepsilon_{hkl} = \frac{d_{hkl} - d_{0,hkl}}{d_{0,hkl}} \tag{1}$$

where d_{hkl}, is the interplanar spacing in the weld for a reflection (hkl).

The stress, σ_{ii}, in each of the three orthogonal directions was found from the strain measurements according to:

$$\sigma_{ii} = \frac{E}{(1+\nu)} \left[\varepsilon_{ii} + \frac{\nu}{(1-2\nu)} (\varepsilon_{11} + \varepsilon_{22} + \varepsilon_{33}) \right] \tag{2}$$

where the Young's modulus, $E = 220\,\text{GPa}$, and Poisson's ratio, $\nu = 0.28$, are the diffraction elastic constants for the $\{211\}$ [30]. $i = 1, 2, 3$ denotes the direction of the lattice spacing measurement and hence, strain and stress direction with respect to the welded plate geometry.

2.3. X-Ray Diffraction

The residual stresses measured using X-rays were performed on an Xstress 3000 instrument using Cr Kα radiation on the $\{211\}$ for the ferrite phase. A 2 mm collimator was used and penetration depths were $<10\,\mu\text{m}$ from the sample surface, along the plane identified in Fig. 2. Stresses in the longitudinal and transverse orientations of the welded plate were inferred through the $\sin^2 \psi$ technique [31]. The ψ angle was varied between -45° and +45° (8 angles in total). Measurements were performed on the as-received welded plates, with no prior grinding or polishing.

3. Results and Discussion

For each of the welded plates, three sets of stress profiles are presented. These include surface stresses measured by neutron diffraction and X-rays. Further measurements were made at 2.5 mm below the surface, to allow comparison with data collected from greater depths below the free surface at other neutron sources using larger gauge volumes. It should be noted that the surface stress results measured by neutron diffraction in this work were volume averaged over 0–0.3 mm below the surface. Macrographs of the three welds, Fig. 4, reveal the layer structure. The boundary between passes is pronounced when LTT-2 is deposited on the HTT filler.

3.1. Surface Stresses - Neutrons

The surface residual stresses measured in three orientations by neutron diffraction are presented in Fig. 5. Larger experimental uncertainties are apparent in the weld metal than the base plate for all three specimens, which

may be attributed to solidification texture. However, trends are evident and symmetry along the centreline would suggest that the data are reliable.

The surface stress profile for Weld L1 (Fig. 5a) shows the characteristic high tensile longitudinal stresses in the HAZ with compression in the weld metal, which is characteristic of these types of LTT alloys and arises as a result of the shape deformation and net expansion following transformation [13]. Conversely, the transverse stresses are tensile in nature in the weld metal and mildly compressive in the HAZ. The normal stresses are compressive in the weld metal. Given their proximity to a free-surface they may be expected to be closer to zero, but it is possible for stress to be retained within a few hundred micrometres of material.

The filler for weld H1 (Fig. 5b) has a sufficiently high M_S that the benefits of transformation plasticity are eradicated on further cooling to ambient temperature and this is reflected by the residual tensile longitudinal stresses in the weld metal. As with weld L1, high tensile longitudinal stresses exist within the HAZ. The transverse stress is tensile in the weld metal and does not display the sharp change to a compressive stress at the fusion boundary, which is evident for weld L1. The normal stress fluctuates about the zero stress mark in both the weld metal and base plate.

Weld L2 (Fig. 5c), which has a capping pass of a highly alloyed LTT filler only, displays a stress profile more akin to weld L1. The longitudinal stress is compressive in the weld metal with high tensile stresses in the HAZ. Continuing the trend of the previous two specimens, tensile transverse stresses are found in the weld metal. The normal stress is generally, mildly tensile but also fluctuates about zero.

The transverse stress measured at the critical location of the weld toe differs significantly between weld L1 ($\sim$ -600 MPa) and weld H1 ($\sim$ -200 MPa). Also, the compressive region for Weld L1 extends further into the base plate and weld metal. The filler M_S clearly influences the transverse residual stress distribution but tension remains in the central portion of the weld metal. This is not the case for the stresses measured in the longitudinal orientation. A possible explanation for this behaviour is that the longitudinally generated stresses are greatest because this is the direction of maximum thermal constraint during cooling. External stresses are known to initiate variant selection during the early stages of the $\gamma \rightarrow \alpha'$ transformation[32]. It is, therefore, presumed that the martensitic variants initially orient themselves in order to cancel the dominant longitudinal stresses. However, as the transformation continues, subsequent variants are less free to align themselves in such a manner as to minimise the tensile stresses in the transverse orientation. This hypothesis may be confirmed by detailed microstructural analysis, however, this is beyond the scope of this paper.

The fusion boundary at the sample surface is the site of greatest interest due to this being the predominant location of failure during fatigue experiments [33]. The residual stresses at the fusion boundary for weld L1 show compression in all orientations. In contrast, the longitudinal stresses in weld

H1 are tensile in nature. The maximum tensile stresses at the fusion boundary for weld L2 are less tensile compared with weld H1, which would suggest that there are benefits to applying an LTT capping pass in multipass welds but not to the extent of a full LTT weld (weld L1).

3.2. Surface Stresses - X-rays

Longitudinal and transverse residual stresses measured with X-rays using the $\sin^2\psi$ method are presented with the surface measurements made with neutrons overlaid in Fig. 6. The error bars from the neutron data have not been included for clarity but can be referred to in Fig. 5. Some of the X-ray results had excessive errors and have been omitted, this may be attributed to solidification texture. Whilst it is useful to compare both the X-ray and neutron data and anticipate similarities, it should be noted that measurements were made with different sampling volumes and at slightly different depths below the surface.

It is broadly apparent that the stresses measured by X-rays and neutrons are in agreement. The X-ray results all display tensile transverse stresses in the weld metal and the effects of using an LTT filler show a reversal of tensile stress (Fig. 6b) to compression (Fig. 6a) in the weld in the longitudinal orientation. The X-ray measurements do not appear to fully replicate the peak longitudinal tensile stresses in the HAZ, which were identified by neutron diffraction. Perhaps the profiles generated by the two techniques may show greater correlation if the number of X-ray measurement locations were to be increased. However, complete agreement between the X-ray and neutron diffraction results cannot be expected due to the difference in measurement depths and sampling volumes.

3.3. Bulk Stresses - Neutrons

The small gauge volume necessary to measure surface stresses deceases the volume of material sampled and therefore, the number of grains. In order to verify the effects of the reduced sampling volume, measurements were made at 2.5 mm below the surface and compared with previously collected data, Fig. 7 [23]. The reduction in sampling volume is significant, 100× for welds L1/L2 and 30× for weld H1. The trends identified for both sets of data for the three welded plates are comparable, the only exception being the extent of compressive stresses measured in the weld metal for weld L2. This is not necessarily a discrepancy because the larger gauge volume will average the strains measured at a depth of 2.5 mm ±1.5 mm, whilst the small gauge volume range is only 2.5 mm ±0.15 mm. This could have a significant effect, depending on the stress gradients in this region. Error bars have been included for the longitudinal orientation and are representative of all orientations for the small gauge volume. Error bars are encompassed within the marker for the large gauge volume measurements. Critically, the stress distributions measured in the vicinity of the surface by both neutrons and X-rays are significantly different to those measured at 2.5 mm below the

surface, with high tensile transverse stresses at the surface in the weld metal being the major differential.

4. Conclusions

Measurement of the surface residual stresses produced following the welding of a series of ferritic steel plates with low transformation-temperature filler alloys has been performed using X-ray and neutron diffraction. From this study the following conclusions and recommendations have been drawn:

- The adoption of a small gauge volume has permitted the measurement of near-surface residual stresses by neutron diffraction. For the first time, this technique has been employed to measure the residual stresses in LTT welds and reveal the local stress variations at the critical fusion boundary location.

- The surface stress distributions measured by neutron diffraction are comparable with those obtained from laboratory X-rays using the $\sin^2\psi$ technique.

- Two LTT welding alloys have been shown capable of inducing compressive longitudinal residual stresses in to the surface layers of the weld metal for multipass welds. Both neutron and X-ray diffraction confirm these findings.

- Tensile transverse stresses were measured in the weld metal for all three welded plates. The stresses became compressive at the fusion boundaries, with weld L1 displaying the greatest levels of compression.

- Weld L1 appears to display the most desirable residual stresses as they are compressive in nature at the fusion boundary, which is the expected site of crack initiation and subsequent propagation during service. In contrast, weld H1, which was produced with a conventional filler alloy, produces tensile longitudinal stresses at the fusion boundary.

- Weld L2, which has a singular capping pass made by an LTT filler, is capable of inducing compressive longitudinal stress in the weld metal near the surface and the stress profile across the fusion boundary appears preferable to weld H1.

Acknowledgments

References

1. D. Löhe, K.-H. Lang, and O. Vöhringer: Handbook of Residual Stress and Deformation of Steel, chap. Residual Stresses and Fatigue Behaviour: ASM International, 2002:27–53.

2. W. K. C. Jones, and P. J. Alberry: 'A model for stress accumulation in steels during welding', *Metals Technology*, 1977, **11**, 557–566.

3. S. Zenitani, N. Hayakawa, J. Yamamoto, K. Hiraoka, Y. Morikage, T. Yauda, and K. Amano: 'Development of new low transformation temperature welding consumable to prevent cold cracking in high strength steel welds', *Science and Technology of Welding and Joining*, 2007, **12**, 516–522.

4. M. C. Payares-Asprino, H. Katsumoto, and S. Liu: 'Effect of martensite start and finish temperature on residual stress development in structural steel welds', *Welding Journal, Research Supplement*, 2008, **87**, 279s–289s.

5. Y. Mikami, Y. Morikage, M. Mochizuki, and M. Toyoda: 'Angular distortion of fillet welded T joint using low transformation temperature welding wire', *Science and Technology of Welding and Joining*, 2009, **14**, 97–105.

6. J. A. Francis, H. J. Stone, S. Kundu, H. K. D. H. Bhadeshia, R. B. Rogge, P. J. Withers, and L. Karlsson: 'Effects of filler metal transformation temperature on residual stresses in a high strength steel weld', *Journal of Pressure Vessel Technology*, 2009, **131**, 0414011–0414018.

7. J. Altenkirch, J. Gibmeler, A. Kromm, T. Kannengiesser, T. Nitschke-Pagel, and M. Hofmann: 'In situ study of structural integrity of low transformation temperature (LTT)-welds', *Materials Science & Engineering A*, 2011, **528**, 5566–5575.

8. T. Kasuya, Y. Hashiba, H. Inoue, T. Nose, K. Ito, and M. Enoki: 'Cold cracking susceptibility of austenitic and martensitic weld metals', *Welding in the World*, 2012, **56**, 76–84.

9. M. Takahashi, and H. Y. Yasuda: 'Variant selection of martensites in steel welded joints with low transformation temperature weld metals', *Journal of Alloys and Compounds*, 2013, **577**, S601–S604.

10. D. L. Saraiva, M. Béreš, C. C. Silva, C. S. Nunes, J. J. M. Silva, and H. F. G. Abreu: 'Application of low m_s temperature consumable to dissimilar welded joint', *Materials Science and Technology*, 2014, , DOI 10.1179/1743284714Y.0000000516.

11. S. H. Thomas, and S. Liu: 'Analysis of low transformation temperature welding (LTTW) consumables – distortion control and evolution of stresses', *Science and Technology of Welding and Joining*, 2014, , DOI 10.1179/1362171814Y.0000000199.

12. J. W. Christian: Theory of Transformations in Metals and Alloys, Part II: 3 ed., Oxford, U. K.: Pergamon Press, 2003.

13. J. A. Francis, H. K. D. H. Bhadeshia, and P. J. Withers: 'Welding residual stresses in ferritic power plant steels', *Materials Science and Technology*, 2007, **23**(9), 1009–1020.

14. S. W. Ooi, J. E. Garnham, and T. I. Ramjaun: 'Low transformation temperature weld filler for tensile residual stress reduction', *Materials and Design*, 2014, **56**, 773–781.

15. A. Ohta, N. Suzuki, Y. Maeda, K. Hiraoka, and T. Nakamura: 'Superior fatigue crack growth properties in newly developed weld metal', *International Journal of Fatigue*, 1999, **21**, S113–S118.

16. J. Eckerlid, T. Nilsson, and L. Karlsson: 'Fatigue properties of longitudinal attachments welded using low transformation temperature filler', *Science and Technology of Welding and Joining*, 2003, **8**, 353–359.

17. H. Lixing, W. Dongpo, W. Wenxian, and Y. Tainjin: 'Ultrasonic peening and low transformation temperature electrodes used for improving the fatigue strength of welded joints', *Welding in the World*, 2004, **48**, 34–39.

18. P. P. Darcis, H. Katsumoto, M. C. Payares-Asprino, S. Liu, and T. A. Siewert: 'Cruciform fillet welded joint fatigue strength improvements by weld metal phase transformations', *Fatigue and Fracture of Engineering Materials and Structures*, 2008, **31**, 125–136.

19. L. Karlsson, and L. Mráz: 'Increasing fatigue life with low transformation temperature (LTT) welding consumables', *Zváranie svarováni*, 2011, **1–2**, 8–15.

20. C. Miki, and T. Masayuki: 'Fatigue strength improvement of out-of-plane welded joints of steel girder under variable amplitude loading', *Welding in the World*, 2013, **57**, 823–840.

21. A. A. Shirzadi, H. K. D. H. Bhadeshia, L. Karlsson, and P. J. Withers: 'Stainless steel weld metal designed to mitigate residual stresses', *Science and Technology of Welding and Joining*, 2009, **14**, 559–565.

22. R. J. Moat, H. J. Stone, A. A. Shirzadi, J. A. Francis, S. Kundu, A. F. Mark, H. K. D. H. Bhadeshia, L. Karlsson, and P. J. Withers: 'Design of weld fillers for mitigation of residual stresses in ferritic and austenitic steel welds', *Science and Technology of Welding and Joining*, 2011, **16**, 279–284.

23. T. I. Ramjaun, H. J. Stone, L. Karlsson, J. Kelleher, R. J. Moat, J. R. Kornmeier, K. Dalaei, and H. K. D. H. Bhadeshia: 'Effect of inter-pass temperature on residual stresses in multi-pass welds produced using a low transformation temperature filler alloy', *Science and Technology of Welding and Joining*, 2014, **19**, 44–51.

24. A. Kromm, T. Kannengiesser, J. Alenkirch, and J. Gibmeier: 'Residual stresses in multilayer welds with different martensitic transformation temperatures analyzed by high–energy synchrotron diffraction', *Materials Science Forum*, 2011, **681**, 37–42.

25. J. Gibmeier, E. Obelode, J. Altenkirch, A. Kromm, and T. Kannengiesser: 'Residual stress in steel fusion welds joined using low transformation temperature (LTT) filler material', *Materials Science Forum*, 2014, **768–769**, 620–672.

26. W. Steven, and A. G. Haynes: 'The temperature of formation of martensite and bainite in low alloy steels', *Journal of the Iron and Steel Institute*, 1956, **183**, 349–359.

27. L. Clapham, S. White, and R. Rogge: 'Neutron diffraction investigation of fluid end cracking in well stimulation pump fluid ends', *International Journal of Pressure Vessels and Piping*, 2006, **83**, 118–122.

28. M. R. Daymond, and H. G. Priesmeyer: 'Elastoplastic deformation of ferritic steel and cementite studied by neutron diffraction and self-consistent modelling', *Acta Materialia*, 2002, **50**, 1613–1626.

29. J. W. L. Pang, T. M. Holden, and T. E. Mason: 'The development of intergranular strains in a high-strength steel', *Journal of Strain Analysis for Engineering Design*, 1998, **33**, 373–383.

30. B. Eigenmann, and E. Macherauch: 'Röntgenographische untersuchung von spannungszuständen in werkstoffen. teil iii. fortsetzung von matwiss. und werkstofftechn', *Materialwissenschaft und Werkstofftechnik*, 1996, **27**, 426–437.

31. J. Lu: Handbook of Measurement of Residual Stresses: Society for Experimental Mechanics, 1996.

32. S. Kundu, and H. K. D. H. Bhadeshia: 'Transformation texture in deformed stainless steel', *Scripta Materialia*, 2006, **55**, 779–781.

33. L. Karlsson, L. Mráz, H. K. D. H. Bhadeshia, and A. Shirzadi: 'Alloying concepts for low transformation temperature welding consumables', *Biuletyn Instytutu Spawalnictwa*, 2010, **5**, 33–39.

Table 1: Combinations of base plate and weld filler alloys.

Weld	Base Plate	Pass 1	Pass 2	Pass 3
L1	BP700	LTT-1	LTT-1	LTT-1
L2	BP700	HTT	HTT	LTT-2
H1	BP700	HTT	HTT	HTT

Table 2: Compositions (wt %) and calculated M_S of the undiluted welding alloys and base plate.

Material	C	Si	Mn	Cr	Ni	Mo	M_S (°C)
LTT-1	0.01-0.03	0.6-0.8	1.2-1.7	12.5-13.0	5.5-6.5	<0.1	169
LTT-2	<0.02	<1	<2	15-18	6-8	<0.1	87
HTT	0.12	0.65	1.50	0.70	2.80	0.85	372
BP700	0.15	0.29	0.98	0.25	0.043	0.15	447

Table 3: Welding parameters.

Voltage (V)	Current (A)	Shielding gas	Gas flow ($l\,min^{-1}$)	Welding speed ($cm\,min^{-1}$)		
				Pass 1	Pass 2	Pass 3
24.7	∼250	Ar+2%CO_2	18	36	30	23

Table 4: Mechanical properties of the undiluted LTT welding alloy and base plate.

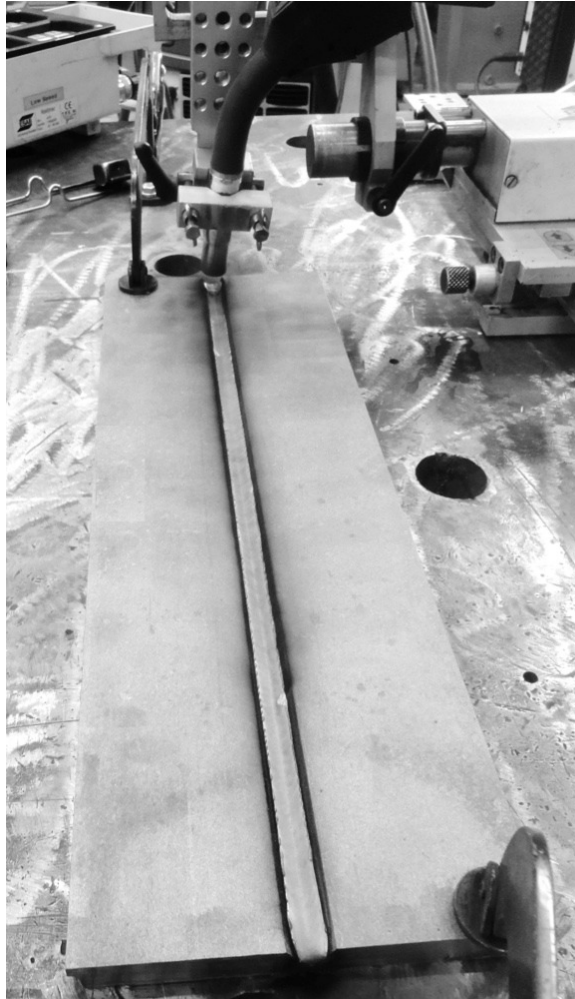| Material	0.2% stress (MPa)	Tensile strength (MPa)	Elongation (%)	Impact energy (at -20°C)
LTT-1	627	1111	14.0	45
LTT-2	316	845	31.8	88
HTT	>900	> 900	19.0	>90
BP700	>700	780-930	14.0	>27

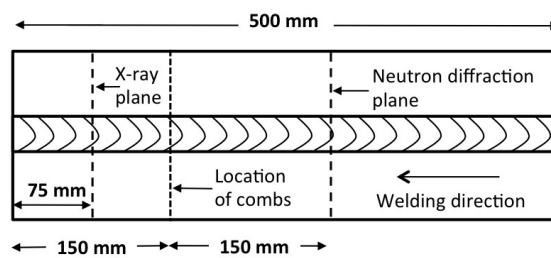Figure 1: Photograph of a weld being produced by automated GMAW.

Figure 2: Plan view of a welded plate showing the locations of the residual strain measurements and reference strain-free specimens.
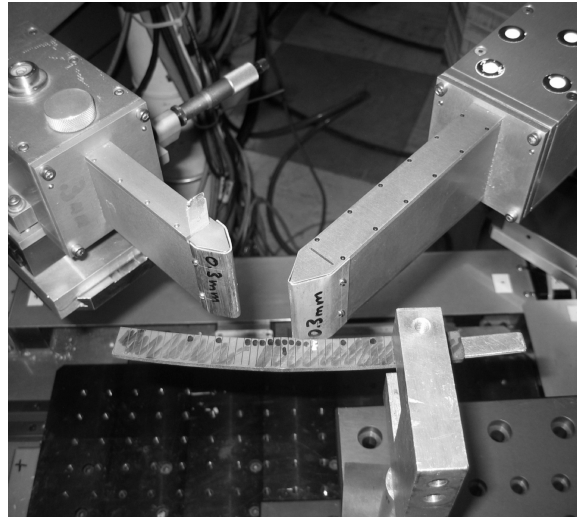
Figure 3: Sectioned 'comb' specimen in-situ, used to determine the strain-free lattice parameter – the presented orientation is for measurement in the normal direction.
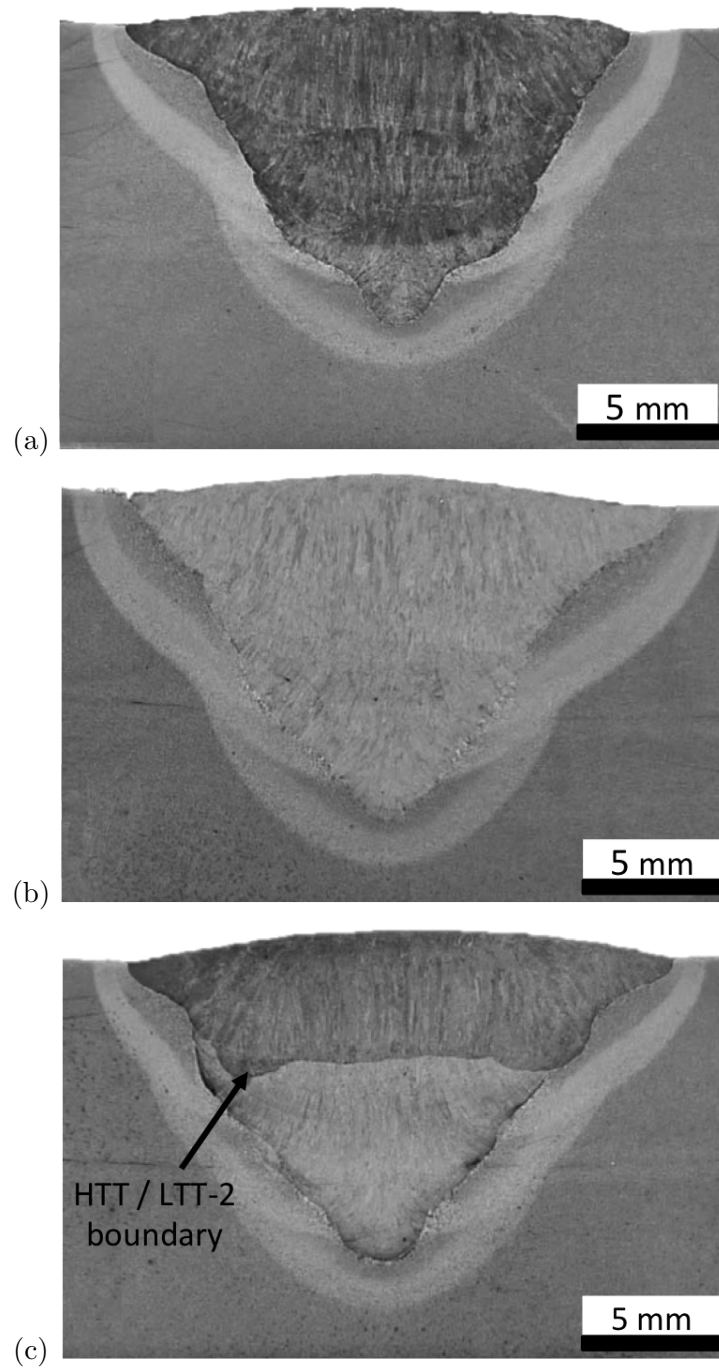
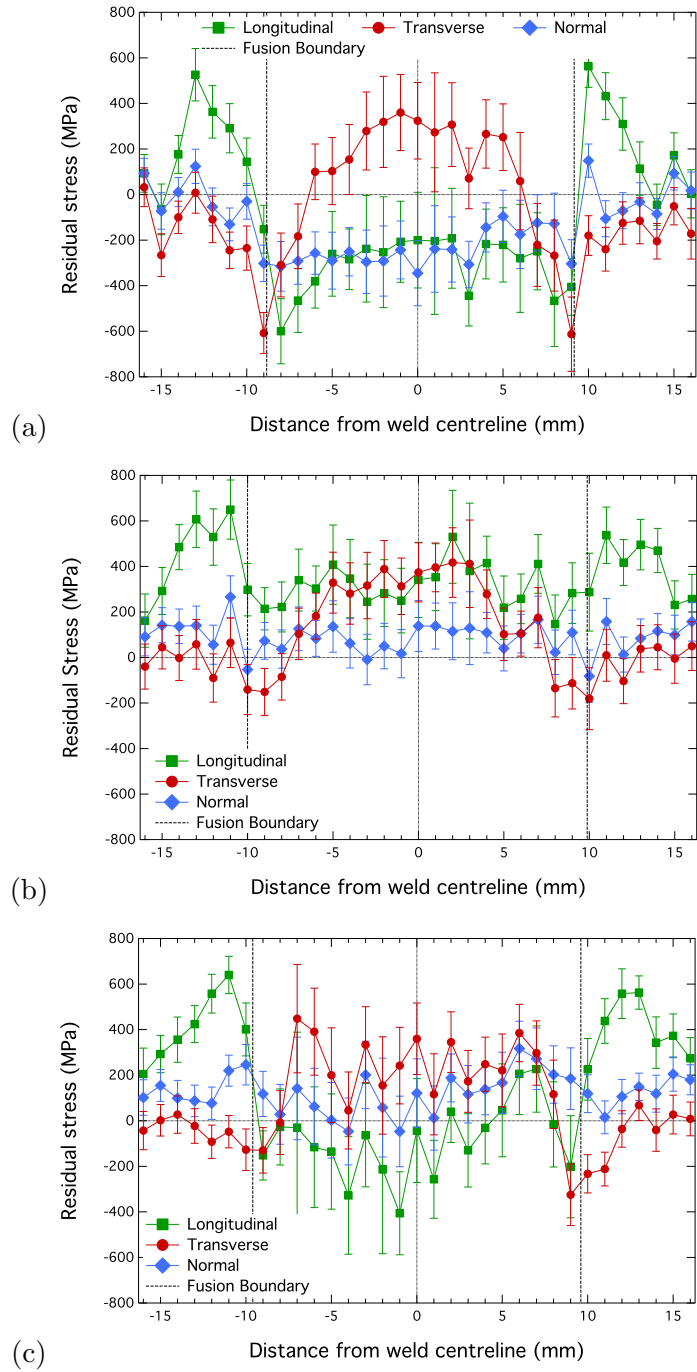Figure 4: Macrostructures of (a) Weld L1, (b) weld H1, (c) weld L2.

Figure 5: Near surface residual stresses measured at a depth of 0.15 mm by neutron diffraction. (a) Weld L1, (b) weld H1, (c) weld L2.
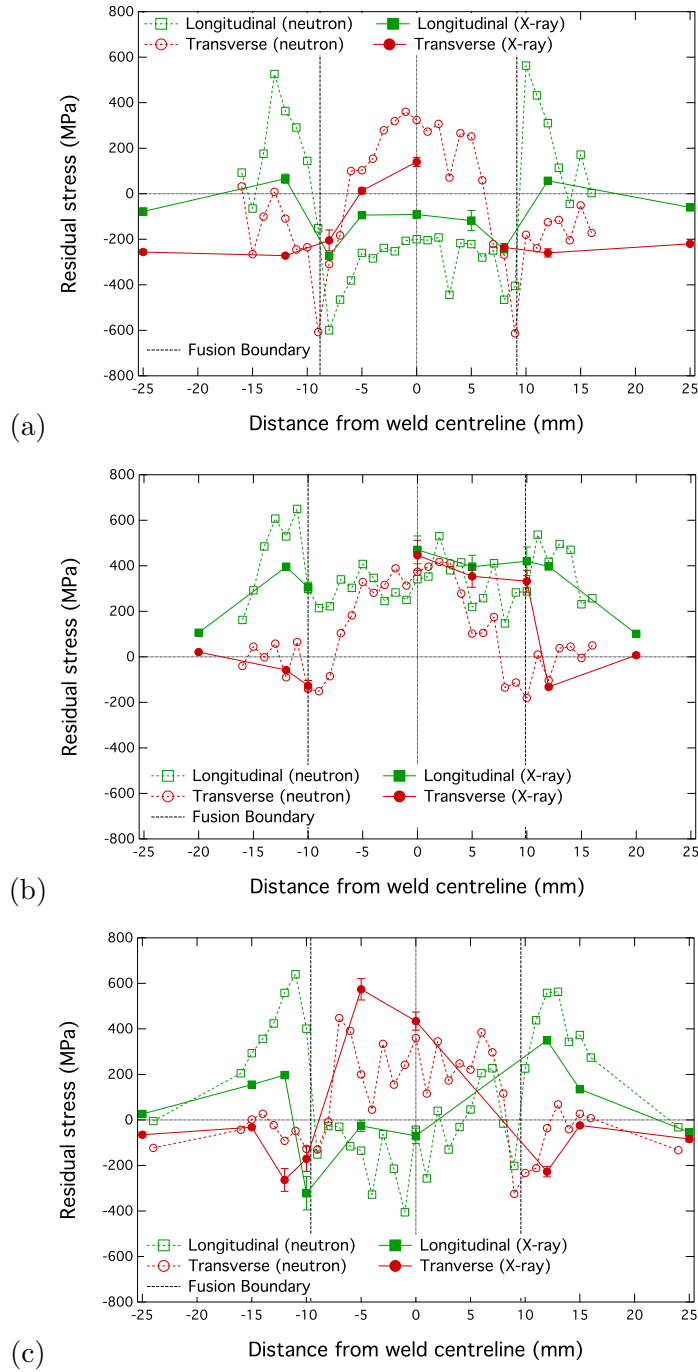
Figure 6: Surface residual stresses measured using X-rays (solid lines) and neutrons (dashed lines). (a) Weld L1, (b) weld H1, (c) weld L2.
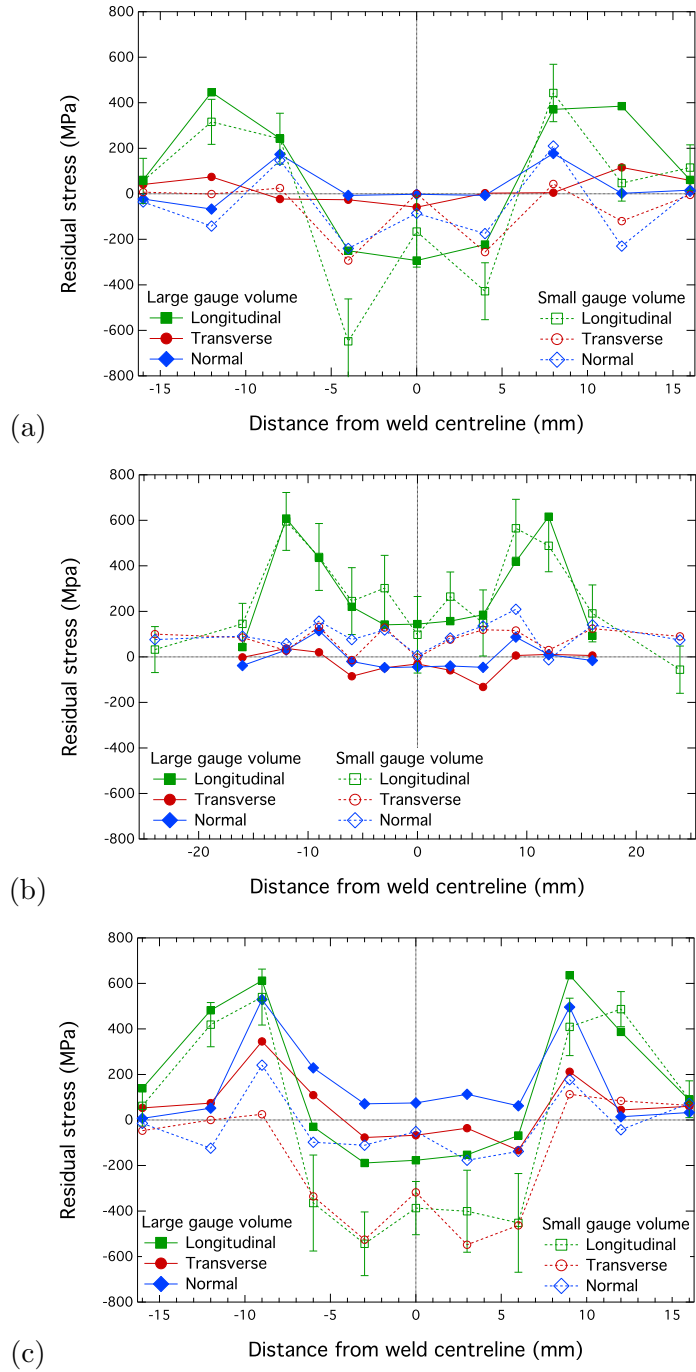
Figure 7: Residual stresses measured using neutrons at a depth of 2.5 mm below the sample surface. Measurements using a large gauge volume [23] (solid lines) and small gauge volume (dashed lines). (a) Weld L1, (b) weld H1, (c) weld L2.